Three-Dimensional Bicontinuous Graphene Monolith from Polymer Templates

Kewei Liu, Yu-Ming Chen, Gina M. Policastro, Matthew L. Becker, and Yu Zhu*

Department of Polymer Science, the University of Akron, 170 University Circle, Akron, Ohio 44325-3909, United States

ABSTRACT The two-dimensional single-layer and few-layered graphene exhibit many attractive properties such as large specific surface area and high charge carrier mobility. However, graphene sheets tend to stack together and form aggregates, which do not possess the desirable properties associated with graphene. Herein, we report a method to fabricate three-dimensional (3D), bicontinuous graphene monolith through a versatile hollow nickel (Ni) template derived from polymer blends. The poly(styrene)/poly(ethylene oxide) were used to fabricate a bicontinuous gyroid template using controlled phase separation. The Ni template was formed by electroless metal depositing on the polymer followed by removing the polymer phase. The resulting hollow Ni structure was highly porous (95.2%). Graphene was then synthesized from this hollow Ni template using chemical vapor deposition and the free-standing bicontinuous graphene monolith was obtained in high-throughput process. Finally, the bicontinuous graphene monolith was used directly as binder-free electrode in supercapacitor applications. The supercapacitor devices exhibited excellent stability.

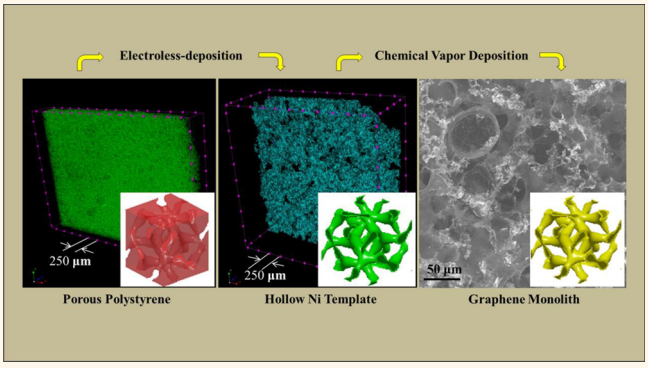

KEYWORDS: graphene · polymer blends · supercapacitor · electroless deposition · bicontinuous

Graphene, as a two-dimensional material with carbon atoms arranged in a hexagonal lattice, exhibits many attractive properties such as extremely high charge carrier mobilities (>200 000 $cm^2/(V \cdot s)$),[1,2] excellent thermal conductivity (>5000 $W/(m \cdot K)$),[3,4] large specific surface area (>2000 cm^2/g),[5,6] and good mechanical properties.[7] Because of those attractive properties, graphene has evolved into a "miracle" material favored by both scientists and engineers, who covet graphene for its unique properties that are not available in other materials.[8,9] The unique properties have expanded efforts for graphene synthesis and fabrication. During the past decade, a number of graphene synthesis and fabrication methods were developed, for instance: mechanical exfoliation of graphite,[2,10] epitaxy-growth on the silicon carbide surface,[11] chemical vapor deposition on metal surfaces,[12−14] solution oxidative exfoliation of graphite,[15,16] longitudinal unzipping carbon nanotube,[17,18] intercalation exfoliation/unzipping of graphite and carbon nanotube,[19−21] and bottom-up synthesis.[22−24] Most methods yield flat, single-layer or few-layered graphene sheets, which are useful for thin-film based applications such as field-effect transistors. However, the integration of graphene sheets into a controlled 3D structure, which are envisioned for electrochemical energy storage electrodes, hydrogen storage median, catalysts and meta-materials,[6,25,26] is still a challenge. The direct use of flat 2D graphene sheets in those applications is limited by two factors: the exfoliated graphene can be restacked, and the connection between the graphene sheets will dramatically diminish the unique properties of the single sheets. Although the synthesis of 3D graphene has been reported[27−32] previously, the connections between graphene sheets are usually not controlled,[29,30] which result in the downgradated properties of 3D graphene. The high-quality CVD graphene grown on the 3D templates[27,28] can provide desired connection, however, the structure and

* Address correspondence to yu.zhu@uakron.edu.

Received for review February 12, 2015 and accepted June 5, 2015.

Published online June 05, 2015
10.1021/acsnano.5b01006

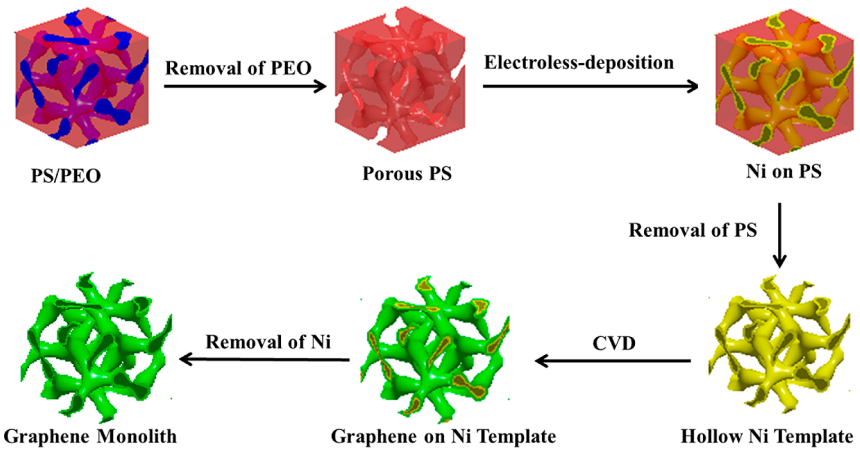

Scheme 1. Schematic illustration of graphene monolith preparation: First, the bicontinuous polymer blends (PS/PEO) were prepared with a twin-screw extruder. Second, the polymer blend was treated with water to remove PEO. The resulting porous PS template was coated with nickel Ni using electroless deposition. Following this step, the PS was dissolved in toluene and the free-standing hollow Ni template was formed. Finally, the graphene was grown on the Ni template by chemical vapor deposition. A free standing, bicontinuous, 3D graphene monolith was obtained after removing the Ni scaffold.

pore-size controls are still missing due to the use of preformed commercial metal foam.[27,28]

In this work, a novel method to fabricate 3D bicontinuous graphene by using versatile polymer templates was demonstrated. The structure and pore size of the graphene can be controlled by corresponding polymer templates. The resulting graphene monolith materials were used in the supercapacitor electrode and exhibited excellent stability (over 6000 cycles with capacity retention of 98%). This work provides a novel way to fabricate high-quality, 3D bicontinuous graphene that can be useful in applications such as electrochemical energy storage electrodes and high surface area catalyst scaffolds.

RESULTS AND DISCUSSION

The fabrication procedure of graphene monolith is illustrated in Scheme 1. First, polystyrene (PS) and poly(ethylene oxide) (PEO) powders were dry-mixed with a twin-screw extruder to form a bicontinuous polymer blend. Second, the polymer blend was treated with water to remove the poly(ethylene oxide). The resulting PS template was coated with Ni by electroless deposition. Following this step, the PS was dissolved in toluene and the free-standing Ni template was formed. Finally, the graphene was grown on the Ni template by chemical vapor deposition. A free-standing, bicontinuous, 3D graphene monolith was obtained after removing the Ni scaffold.

The bicontinuous template in this work was created by the simple polymer blending method. When two immiscible polymers (PS and PEO) are mixed in the melting state and are then cooled down, they will experience phase separation. If the volume fraction of polymer **I** is significantly less than 1.0, the discrete droplets of polymer **I** will disperse in the continuous polymer **II** matrix. With the increase of the volume fraction of polymer **I**, the blend will eventually form an inversion phase, with the original matrix polymer **II** becoming droplets and the original dispersed polymer **I** phase becoming continuous. When the volume fraction gets close to the inversion point, a bicontinuous gyroid structure is observed.[33] However, these structures are in nonequilibrium states and will disappear after a coarsening process. Nonetheless, recent studies have shown that the bicontinuous structure is maintained through rapid freezing.[34−36] To generate the porous structure, two polymer components with different solubility are required. On the basis of these two requirements (immiscible polymers with different solubilities), water-soluble poly(ethylene oxide) and organic solvent soluble polystyrene were used. A mini twin-screw extrusion compounder was used to prepare the polymer blends. The resulting polymer blends were cooled in air after they were collected. Thereafter, the polymer blends were pressed to form thin films. PEO was removed by soaking in warm water (60 °C). After this process, the bicontinuous 3D polystyrene templates were prepared. The details of sample preparation are described in the Methods section.

The morphology of polymer blends can be affected by many parameters such as the polymer components used, molecular weights of the polymers, mass ratio and processing conditions.[37] In this work, several key parameters of the chosen polymer blends (PS/PEO) were studied to control the morphology of the final porous template. It has been described in previous work that the viscosity of the polymer can greatly affect the morphology of the blends. When the viscosities of the two polymers are similar, the polymers can be finely dispersed and the coalescence is delayed.[37,38] PS:PEO blends system has been explored by several groups.[39,40] The complex viscosities of the PS and PEO were found to be very close at the elevated temperature,

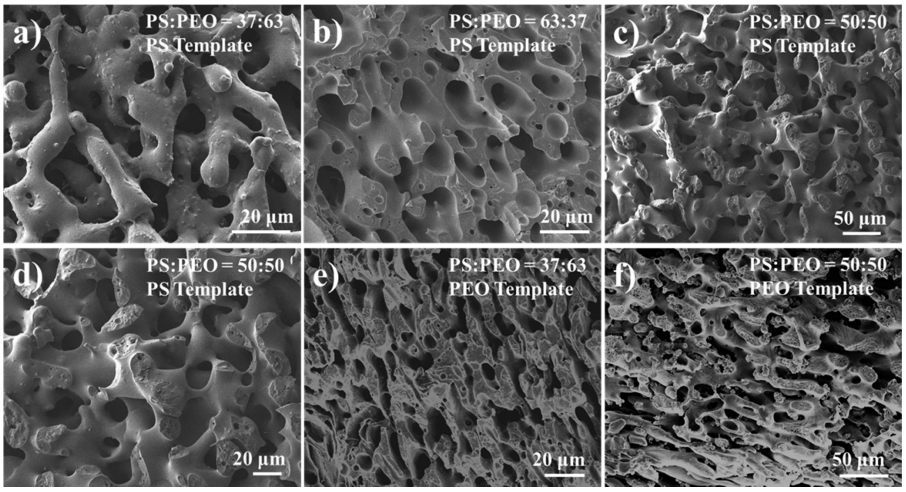

Figure 1. SEM images of the polymer templates obtained from different mass ratio of PS and PEO. (a) The PS template obtained from the blend with PS:PEO = 37:63. (b) The PS template obtained from the blend with PS:PEO = 63:37. (c and d) The PS template obtained from the blend with PS:PEO = 50:50 under different magnification. (e) The PEO template obtained from the blend with PS:PEO = 37:63. (f) The PEO template obtained from the blend with PS:PEO = 50:50. The continuous PS and PEO templates were obtained when the ratios of PS:PEO were 37:63 or 50:50. When the ratio of PS:PEO was 63:37, only continuous PS template was obtained.

which is beneficial for forming a bicontinuous phase in a wider range of PS/PEO mass ratio. The complex viscosities of the polymers used in this work were measured (Supporting Information Figure S1). The results indicate that the viscosities of the two polymers are similar at the blending temperature (170 °C) with high shear-rate. As the blend of PS and PEO is in a nonequilibrium state, a spontaneous phase separation will occur once blending is stopped. To preserve the interpenetrated structure of PS/PEO, the blend must be rapidly cooled below the glass transition temperature of one component immediately following intensive mixing.[41] The thermal properties of polymers used in this work were studied and the results indicated the glass transition temperature of PS (based on the differential scanning chromatography in Supporting Information, Figure S2) and PEO (based on the data from commercial supplier) are ~73 and ~−67 °C, respectively. This suggests that quenching the polymer blend in air can freeze PS, leaving the structure of the polymer blend intact. We studied the morphology of the PS template obtained by air quenching and liquid nitrogen quenching (Supporting Information Figure S3). The results confirmed that quenching the samples in air and liquid nitrogen had similar effects. Thus, the samples used in this work were quenched in air, which is easier to control than cryogenic quenching.

The morphology of the polymer blends structure is dependent on the mass ratio of the polymers. In this work, PS/PEO blends with mass ratios of 37:63, 50:50, and 63:37 were prepared. The polymer blends were further treated with water or toluene, in order to remove the PEO or PS, respectively. Figure 1 shows SEM images of the PS and PEO templates prepared with different mass ratio. For the PS templates, the pore size is 24.1 ± 2.2 μm (PS:PEO = 37:63, Figure 1a), 11.7 ± 1.5 μm (PS:PEO = 63:37, Figure 1b), and 16.3 ± 1.5 μm (PS:PEO = 50:50, Figure 1c,d). The bicontinuous properties of the polymer templates can be verified by preparing inversed PEO templates and the continuity of PS/PEO blends was probed quantitatively by selective solvent extraction (Supporting Information Figure S5). In this study, the polymer blends were treated with toluene and the porous PEO templates were obtained. As shown in Figure 1e,f, the polymer blends with a mass ratio of 37:63 and 50:50 (PS:PEO) formed porous PEO templates. However, for the blend with a mass ratio of 63:37 (PS:PEO), a PEO template broke during the etching process. The results suggest that the template obtained in blended systems with mass ratios of 37:63 and 50:50 are bicontinuous. In this work, the PS template (Figure 1c,d) from the blends with PS/PEO mass ratio of 50:50 was utilized for the remaining studies due to the relative small pore size.

To grow graphene as illustrated in Scheme 1, the graphene growth substrate (such as Ni[14] or Cu[12,13]) needs to be prepared on the surface of the templates. Because the polymer template is porous and nonconductive, conventional film-forming techniques, such as e-beam evaporation, sputter-coating or electrical plating, cannot provide homogeneous metal coatings on the surface of the templates. Therefore, the metal (Ni) was deposited onto the polymer templates *via* electroless plating. Because the conventional Ni electroless plating is usually carried out at 90 °C in aqueous solution,[42] the PS template was chosen for the deposition of Ni. However, initial experiments showed that this temperature (90 °C) is too high compared with the T_g of the PS (73 °C), which led to the movement of polymer molecules, destroying the bicontinuous

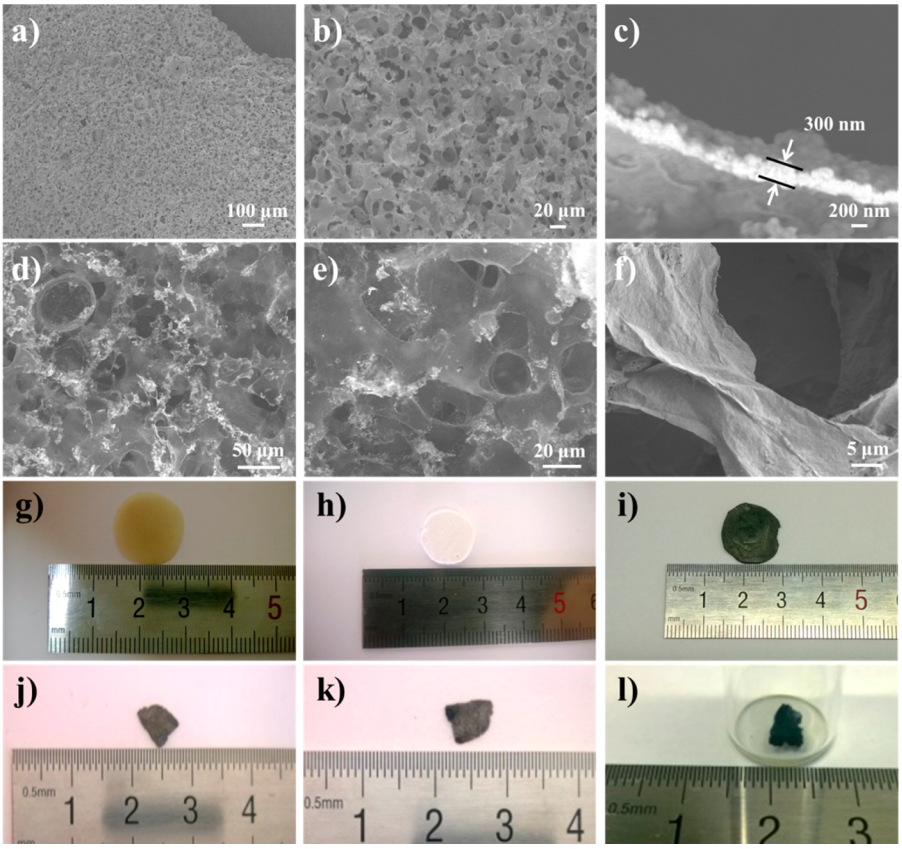

Figure 2. Optical and SEM images of bicontinuous porous structures fabricated in this work. (a−c) SEM images of the porous Ni templates; (d−f) SEM images of the graphene monolith. (g) Optical image of polymer blends (PS/PEO) film. (h) Optical image of PS film after removing PEO. (i) Optical image of electroless Ni template. (j) The small Ni sample from electroless Ni template in (i). The Ni template was cut into smaller pieces in order to fit the size of the sample holder in the CVD furnace. (k) The graphene covered Ni template after CVD growth. The sample kept its original shape, even after CVD process. (l) The graphene monolith sample. The sample was obtained by removing Ni and stored in a glass vial.

porous structure. As such, a modified electroless deposition is used to coat Ni film on the PS template. In this method, the porous PS templates were immersed in palladium chloride ($PdCl_2$) solution, where palladium (Pd) ions can be absorbed onto the surface of PS. The treated PS template was immersed into the electroless Ni solution. During this step, the absorbed Pd ions were reduced to Pd clusters, which act as catalysts. The Ni ions in the solution were able to be reduced to Ni on the surface of the PS template at a lower temperature (60 °C).[43] The reduced Ni on the PS surface also acts as the catalytic center for the following deposition process, allowing Ni film to be homogeneously deposited on the surface of PS template. The details of the electroless deposition of Ni on the PS template are described in the Methods section.

The free-standing Ni template was obtained after removing the polystyrene with hot toluene. As shown in Figure 2a−c, the porous hollow Ni template structure is similar to the PS template. It is worth noting that this Ni template is different from the commercial Ni foam used in previous publications.[27,44,45] The Ni template in this work is hollow and the thickness of the Ni film is in the order of a few hundreds of nanometers (Figure 2c). In comparison, the commercial Ni foam consists of solid Ni branches. Graphene was grown on the surface of the hollow Ni templates by using low-pressure chemical vapor deposition.[13,14,44,45] Acetylene was used as the carbon source for the graphene growth and the detailed experiments are described in the Methods section. The Ni template was removed *via* aqueous etchant allowing for the fabrication of a free-standing graphene monolith (see Methods section for the details). Figure 2d−f shows SEM images of free-standing graphene. Those images indicate that the graphene monolith has similar bicontinuous porous structure compared to the Ni template. Panels g−l of Figure 2 are optical images of templates/porous materials prepared in this work. The polymer blends were compressed into disks as shown in Figure 2g. This pale-yellow sample was treated with water to remove the PEO and obtain the white PS disk sample in Figure 2h. The PS disk sample was coated with Ni by electroless deposition and then PS was removed by organic solvent leaching, resulting in the black Ni disk sample in Figure 2i. The Ni disk was cut into smaller pieces (Figure 2j) in order to fit the size of CVD tube furnace. The graphene covered Ni template following CVD

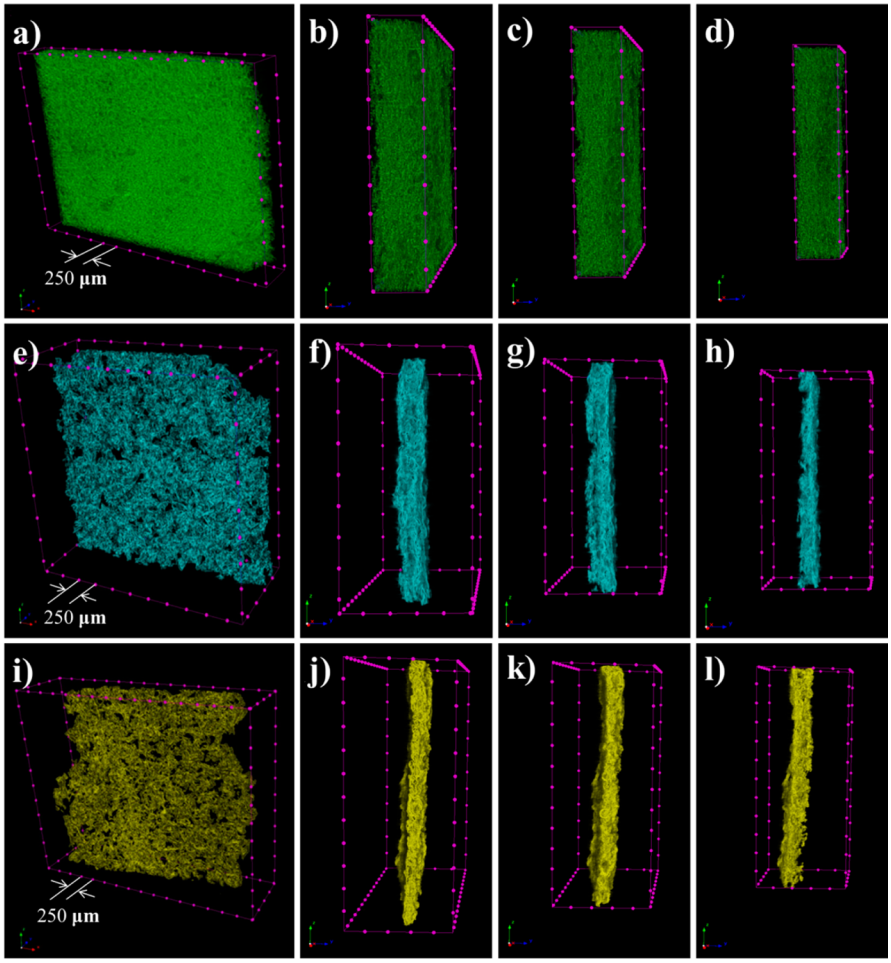

Figure 3. X-ray microcomputed tomography reconstructed images of bicontinuous templates. (a−d) Bicontinuous PS templates. (e−h) Bicontinuous hollow Ni templates (i−l) Bicontinuous graphene on Ni templates. The cross-section images of different templates (a, e, and i) at indicated location are shown in the right of the reconstructed images. The porosities of PS template, Ni template, and graphene covered Ni template are 62.1%, 95.2%, and 94.0%, respectively.

growth is shown in Figure 2k. Finally, the Ni was removed. The resulting lightweight graphene monolith is shown in Figure 2l. It is clear that this procedure allows for the fast fabrication of large graphene samples with good yield.

To further characterize the bicontinuous structure obtained from the polymer blends system, X-ray microcomputed tomography (μCT) was used. In this study, the sample was mounted on the rotating stage with a microfocus X-ray source. The projection images were captured by a planar multichannel X-ray detector. From these 2D shadow projection images, the structures of the templates were reconstructed. The reconstructed images are shown in Figure 3. The video presentations of the reconstructed templates are shown in Supporting Information (SI video S−S3). Figure 3a−d shows the reconstructed PS templates. The structures are similar to those observed in SEM, and the cross-section images indicated that the template has a bicontinuous structure. The porosity of the PS template is 62.1%, which is larger than the theoretical portion (~50%) of PS in the blends. This difference may originate from the weak X-ray absorption of polymeric materials, which results in the blurred interfaces between the polymer and void space, inhibiting the accurate calculation of the porosity. Figures 3e−h and 3i−l are Ni templates and graphene covered Ni templates, respectively. Their images are sharp compared to the PS template. The porosity of the Ni template is 95.2%, which confirms that it is a highly porous, hollow structure. The porosity of graphene covered Ni sample is 94.0%; therefore, the volume faction of graphene is about 1.2%. On the basis of this value, the free-standing graphene monolith is highly porous (porosity over 98.8%) and bicontinuous. The free-standing graphene monolith samples were measured by μCT; however, the intensity of the signal was too weak for reconstruction.

Although Ni has been used as a graphene growth substrate, most reports use evaporated Ni film or Ni foil.[17,18] As far as we know, there is no report for growing graphene on electroless Ni. The energy-dispersive X-ray spectrometer (EDX) (Supporting Information Figure S4) indicates a small amount of phosphorus

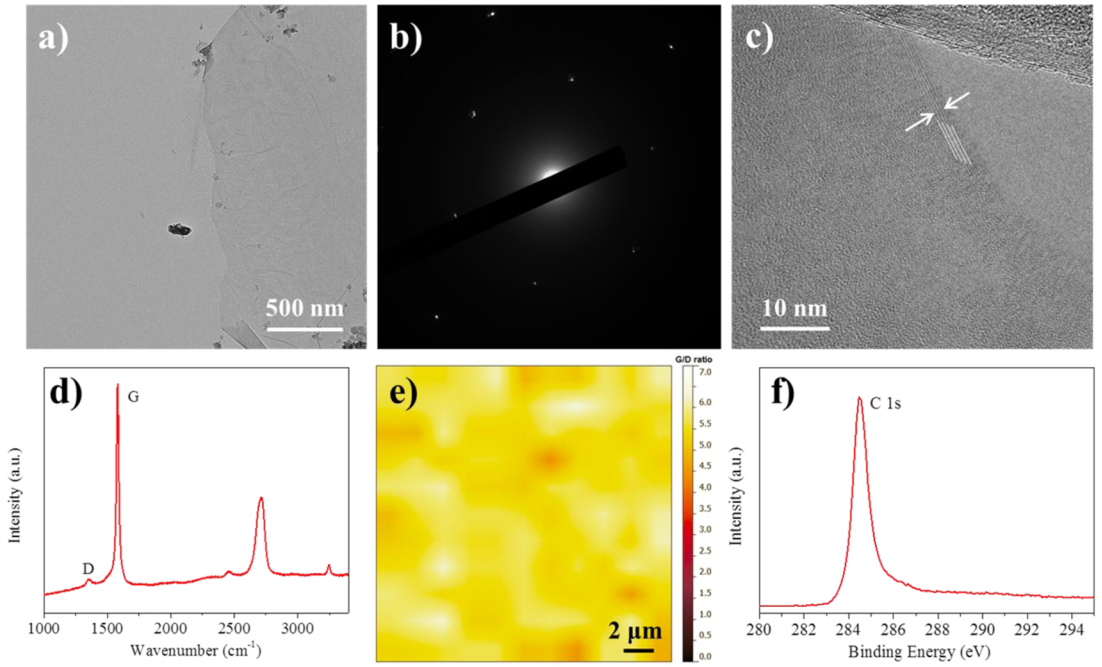

Figure 4. Characterization of graphene formed on the electroless Ni substrates. (a) TEM image of graphene piece from free-standing graphene monolith. (b) The electron diffraction pattern of graphene. (c) High-resolution TEM image shows that the graphene is multilayered. (d) The typical Raman spectrum of free-standing graphene monolith. (e) Raman mapping of graphene grown on the flat electroless Ni substrate. (f) High-resolution XPS C 1s spectrum of graphene monolith.

existing in the free-standing Ni templates even after thermal annealing. This phosphorus is a result of the electroless deposition process.[43] Thus, the quality of the graphene on the electroless Ni needs to be investigated. Figure 4a–c shows TEM images of free-standing graphene monolith. The graphene formed on electroless Ni are typically multilayered, which is similar to those formed on the Ni film or foil. The diffraction pattern in Figure 4b was typically observed, although multiple sets of hexagonal diffraction spots were also quite common. The typical Raman spectrum of graphene monolith is shown in Figure 4d. The small D peak implies that the quality of the graphene is comparable to that formed from other Ni sources.[14] The ratio of G/2D peak is much larger than 1:1, which is typical for multilayered graphene. This result agrees well with the TEM images in Figure 4c. Because the graphene monolith has a curved surface and porous structure, it is difficult to use Raman mapping to evaluate the quality of the graphene in a large area. To further study the homogeneity of the graphene formed on the electroless Ni, an electroless Ni film was prepared on a flat quartz substrate using the same procedure as for the PS template. The graphene was grown onto the electroless Ni covered quartz sample in the same method used for the porous Ni template. The Raman mapping of graphene grown on electroless Ni covered quartz was performed, on which 121 points were measured in a 20 $\times$ 20 μm^2 area. As shown in Figure 4e, the ratio of G/D is plotted and most areas (light colored) have large G/D value. This result confirmed that the fabrication of homogeneous, high-quality graphene can be done by deposition on an electroless Ni surface. The graphene monolith formed in this work was characterized by X-ray photoelectron spectroscopy (XPS). The C 1s spectrum (Figure 4f) indicates that most carbon atoms form carbon–carbon bonds. The concentration of carbon is 97.1% in graphene monolith.

Due to the high porosity, bicontinuous structure and good conductivity, the graphene monolith can be directly used as an electrode for electrochemical energy storage applications. Supercapacitors based on the graphene monolith material were fabricated, and the performance of the devices was tested. The results are shown in Figure 5. Additional information for the device fabrication and testing methods are shown in the Supporting Information. The supercapacitor devices worked properly up to 3.5 V, and the energy density reached 34.05 Wh/kg. The specific capacitance of the electrode was 80 F/g, which corresponded to the effective specific electrochemical surface area of 389 m^2/g.[25,46] (Supporting Information, specific electrochemical surface area). The capacitance retention after 6000 cycles was 98%. This can be attributed to the high sp^2 carbon content in the graphene monolith which leads to the long-cycle stability of the device. The electrochemical performance of graphene monolith electrode and other porous graphene based electrodes was summarized (Supporting Information Table S1). Although this work does not focus on the performance of the supercapacitor, the results indicated

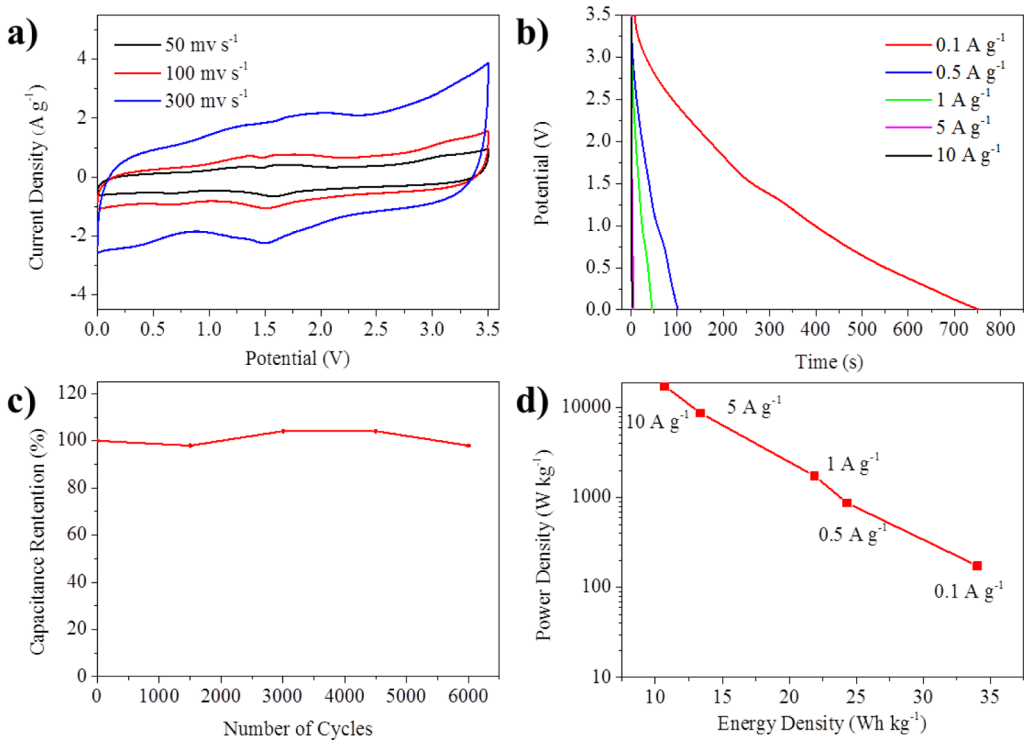

Figure 5. Characterization of graphene monolith based supercapacitors. (a) Cyclic voltammograms of graphene monolith based supercapacitor. The CV results indicate that the capacitor can be operated in a voltage range of 3.5 V. (b) The discharge curves of the supercapacitors based on the galvanostatic tests under different current density. (c) The cycling test of the supercapacitor indicates the capacitance retention is 98% after 6000 cycles. (d) The Ragone plot of the supercapacitors fabricated in this work. The energy density of the capacitor reaches 34.05 Wh/kg.

that the energy density of the graphene monolith based supercapacitor is very competitive and the cycling performance is among the best reported results.

CONCLUSION

In previous reports of growing high quality 3D CVD graphene, the porous templates are usually formed by commercial porous inorganic materials such as Ni foam and anodic alumina tubes.[27,28,47] The structure and pore-size control of the templates are very limited. In this report, for the first time, the porous graphene growth substrate was prepared from a polymer blend template. With a polymer blend as the template material, the control and modification of the structure is made easier, while the cost of templates was significantly reduced as well. The bicontinuous graphene monolith was successfully prepared and supercapacitors with the binder-free graphene monolith electrode were demonstrated. In addition, this work also systematically investigated the electroless Ni as a novel graphene growth substrate. The success of using electroless Ni as graphene growth substrate provides a universal way to synthesize high quality graphene on porous templates.

METHODS

Preparation of Polymer Blends. PS (MW 45 000 g/mol) and PEO (MW 200 000 g/mol) used in this work were purchased from Scientific Polymer Products, Inc. A mixture of 6.5 g of PS polymer and PEO powders was preblended mechanically, then added to a corotating twin screw extruder (MiniLab HAAKE Rheomex CTW5, Germany) at a rotation rate of 20 rpm and a temperature of 170 °C. After feeding, the polymer blends were blended at 200 rpm and 170 °C under the protection of N_2 for 10 min. Polymer blends were extruded at 20 rpm and cooled in air to freeze the nonequilibrium state. Polymer sample disks were prepared by pressing the sample with heated glass slides. The beaded samples were compressed between two aluminum foil sheets, under 20 psi for 2 min at 150 °C, followed by dropping cold water on aluminum foil for 2 min to help remove sample off. After compressing, a disk was formed with a thickness of approximately 0.2 mm. Porous PS templates were obtained by removing PEO phase with water extraction for 3 days.

Nickel Deposition. The porous PS templates were immersed into an activating solution mixed with ethanol (45 mL), HCl (1 N, 5 mL), and $PdCl_2$ (0.05 g) at room temperature for 4 h. Then, the Pd-activated PS templates were immersed in to the Ni electroless plating solution (purchased from Caswell, Inc.) at a temperature of 55−60 °C for 40−50 min. To remove PS, the Ni coated samples were immersed into hot toluene (80 °C) for 15 h.

Preparation of Graphene Monolith. The as-prepared Ni template was placed in a ceramic combustion boat (4 cm × 0.5 cm × 0.8 cm), then inserted into a quartz tube with a diameter of 1.91 cm. The quartz tube with Ni template inside was loaded into the cold zone of a tube furnace for graphene growth. The tube furnace was evacuated and purged with argon three times. Then, the hydrogen (64 sccm) and argon (100 sccm) were introduced into the furnace and the furnace was heated to 700 °C. After the temperature in the furnace was stable, argon

was stopped and the Ni template was loaded into the hot region without breaking vacuum. The sample was annealed for 5–10 min at 700 °C before the carbon feedstock (acetylene) was introduced to the system. The graphene growth time was between 3 and 5 min at 700 °C (pressure = 26.66 Pa, acetylene flow rate = 4 sccm). After growth, the sample was immediately unloaded into the cold zone without breaking vacuum. The sample was removed from the CVD furnace after the temperature reached room temperature. The Ni template was removed with the etching solution (1 M HCl/1 M $FeCl_3$) at 80 °C for 4 h. After carefully washing with deionized water, the free-standing graphene monolith was obtained by freeze-drying the samples for 2 days. Metal residues from Ni templates and etching solutions were removed by annealing graphene monolith at 1000 °C in a tube furnace with H_2 (100 sccm) and Ar (20 sccm) under vacuum for 10 min.

X-ray Tomography Characterization. PS templates, porous Ni, and graphene covered Ni samples were loaded in a Skyscan 1172 μCT for μCT experiments. Samples containing Ni were scanned with a 0.5 mm Al filter at 59 kV, 169 μA, and 10 W. The contrast of PS templates under X-ray were weak; therefore, they were scanned without a filter at 47 kV, 213 μA, and 10 W. Each sample was scanned at 1.7 μm pixels using a medium camera. 2D μCT scans were reconstructed in NRecon and analyzed in CTan for porosity data.

Supercapacitor Fabrication and Testing. Graphene monolith was fabricated into a symmetric two-electrode electric double-layer capacitor following our previous work.[43] To prepare the device, free-standing graphene monolith was directly used as the electrode without binder materials. A polytetrafluoroethylene (PTFE) membrane was used as the separator. The electrolyte was prepared by mixing 1 M lithium hexafluorophosphate ($LiPF_6$, Oakwood Chemical) acetonitrile solution and 1-butyl-1-methylpyrrolidinium tetrafluoroborate ($PYR_{14}BF_4$, Ionic Liquids Technologies) with volume ratio of 1:1. The electrochemical tests were carried out by using a CHI electrochemical workstation (CHI 608E).

Characterization. Image characterizations were collected by a JEOL-7401 Field Emission Scanning Electron Microscope, a Hitachi TM-3000 Tabletop Microscope equipped with an energy-dispersive X-ray spectrometer (EDX), a FEI Scanning Transmission Electron Microscope and a FEI Tecnai TF20 FEG transmission electron microscope for high resolution analysis. Raman spectroscopy was recorded in a HORIBA LabRAM HR High-Resolution Raman Microscope System. The X-ray microcomputed tomography was carried out on a Bruker SkyScan 1172 microcomputed tomography. The X-ray Photoelectron Spectrometer was obtained from PHI VersaProbe II Scanning XPS Microprobe. The pore size of the polymer template was calculated based on the SEM images by using JEOL SMile View software.

Conflict of Interest: The authors declare no competing financial interest.

Acknowledgment. The authors thank Dr. B. Wang for help with the SEM and TEM, Dr. M. Gao from Kent State University for the high resolution TEM characterization, Dr. N. Zhorro from the National Polymer Innovation Center for help with the XPS characterization, E. Laughlin for technical support. K. Liu, Y. Chen and Y. Zhu are grateful for financial support from University of Akron, National Science Foundation (NSF) through NSF-CBET 1505943 and ACS Petroleum Research Fund (PRF# 53560 -DNI 10). G. M. Policastro is grateful for a fellowship from RA Helms.

Supporting Information Available: The reconstructed videos (.avi) of X-ray microcomputed tomography of the polymer templates, Ni template and graphene covered Ni template; the detailed electrochemical tests and additional figures. The Supporting Information is available free of charge on the ACS Publications website at DOI: 10.1021/acsnano.5b01006.

REFERENCES AND NOTES

1. Bolotin, K. I.; Sikes, K. J.; Jiang, Z.; Klima, M.; Fudenberg, G.; Hone, J.; Kim, P.; Stormer, H. L. Ultrahigh Electron Mobility in Suspended Graphene. *Solid State Commun.* **2008**, *146*, 351–355.
2. Novoselov, K. S.; Geim, A. K.; Morozov, S. V.; Jiang, D.; Zhang, Y.; Dubonos, S. V.; Grigorieva, I. V.; Firsov, A. A. Electric Field Effect in Atomically Thin Carbon Films. *Science* **2004**, *306*, 666–669.
3. Balandin, A. A.; Ghosh, S.; Bao, W.; Calizo, I.; Teweldebrhan, D.; Miao, F.; Lau, C. N. Superior Thermal Conductivity of Single-Layer Graphene. *Nano Lett.* **2008**, *8*, 902–907.
4. Pop, E.; Mann, D.; Wang, Q.; Goodson, K.; Dai, H. Thermal Conductance of an Individual Single-Wall Carbon Nanotube above Room Temperature. *Nano Lett.* **2005**, *6*, 96–100.
5. Peigney, A.; Laurent, C.; Flahaut, E.; Bacsa, R. R.; Rousset, A. Specific Surface Area of Carbon Nanotubes and Bundles of Carbon Nanotubes. *Carbon* **2001**, *39*, 507–514.
6. Zhu, Y.; Murali, S.; Stoller, M. D.; Ganesh, K. J.; Cai, W.; Ferreira, P. J.; Pirkle, A.; Wallace, R. M.; Cychosz, K. A.; Thommes, M.; et al. Carbon-Based Supercapacitors Produced by Activation of Graphene. *Science* **2011**, *332*, 1537–1541.
7. Lee, C.; Wei, X.; Kysar, J. W.; Hone, J. Measurement of the Elastic Properties and Intrinsic Strength of Monolayer Graphene. *Science* **2008**, *321*, 385–388.
8. Geim, A. K. Graphene: Status and Prospects. *Science* **2009**, *324*, 1530–1534.
9. Geim, A. K.; Novoselov, K. S. The Rise of Graphene. *Nat. Mater.* **2007**, *6*, 183–191.
10. Novoselov, K. S.; Geim, A. K.; Morozov, S. V.; Jiang, D.; Katsnelson, M. I.; Grigorieva, I. V.; Dubonos, S. V.; Firsov, A. A. Two-Dimensional Gas of Massless Dirac Fermions in Graphene. *Nature* **2005**, *438*, 197–200.
11. Berger, C.; Song, Z.; Li, X.; Wu, X.; Brown, N.; Naud, C.; Mayou, D.; Li, T.; Hass, J.; Marchenkov, A. N.; et al. Electronic Confinement and Coherence in Patterned Epitaxial Graphene. *Science* **2006**, *312*, 1191–1196.
12. Li, X.; Cai, W.; An, J.; Kim, S.; Nah, J.; Yang, D.; Piner, R.; Velamakanni, A.; Jung, I.; Tutuc, E.; et al. Large-Area Synthesis of High-Quality and Uniform Graphene Films on Copper Foils. *Science* **2009**, *324*, 1312–1314.
13. Sun, Z.; Yan, Z.; Yao, J.; Beitler, E.; Zhu, Y.; Tour, J. M. Growth of Graphene from Solid Carbon Sources. *Nature* **2010**, *468*, 549–552.
14. Reina, A.; Jia, X.; Ho, J.; Nezich, D.; Son, H.; Bulovic, V.; Dresselhaus, M. S.; Kong, J. Large Area, Few-Layer Graphene Films on Arbitrary Substrates by Chemical Vapor Deposition. *Nano Lett.* **2008**, *9*, 30–35.
15. Dikin, D. A.; Stankovich, S.; Zimney, E. J.; Piner, R. D.; Dommett, G. H. B.; Evmenenko, G.; Nguyen, S. T.; Ruoff, R. S. Preparation and Characterization of Graphene Oxide Paper. *Nature* **2007**, *448*, 457–460.
16. Marcano, D. C.; Kosynkin, D. V.; Berlin, J. M.; Sinitskii, A.; Sun, Z.; Slesarev, A.; Alemany, L. B.; Lu, W.; Tour, J. M. Improved Synthesis of Graphene Oxide. *ACS Nano* **2010**, *4*, 4806–4814.
17. Kosynkin, D. V.; Higginbotham, A. L.; Sinitskii, A.; Lomeda, J. R.; Dimiev, A.; Price, B. K.; Tour, J. M. Longitudinal Unzipping of Carbon Nanotubes To Form Graphene Nanoribbons. *Nature* **2009**, *458*, 872–876.
18. Cano-Márquez, A. G.; Rodríguez-Macías, F. J.; Campos-Delgado, J.; Espinosa-González, C. G.; Tristán-López, F.; Ramírez-González, D.; Cullen, D. A.; Smith, D. J.; Terrones, M.; Vega-Cantú, Y. I. Ex-MWNTs: Graphene Sheets and Ribbons Produced by Lithium Intercalation and Exfoliation of Carbon Nanotubes. *Nano Lett.* **2009**, *9*, 1527–1533.
19. Behabtu, N.; Lomeda, J. R.; Green, M. J.; Higginbotham, A. L.; Sinitskii, A.; Kosynkin, D. V.; Tsentalovich, D.; Parra-Vasquez, A. N. G.; Schmidt, J.; Kesselman, E.; et al. Spontaneous High-concentration Dispersions and Liquid Crystals of Graphene. *Nat. Nanotechnol.* **2010**, *5*, 406–411.
20. Kosynkin, D. V.; Lu, W.; Sinitskii, A.; Pera, G.; Sun, Z.; Tour, J. M. Highly Conductive Graphene Nanoribbons by Longitudinal Splitting of Carbon Nanotubes Using Potassium Vapor. *ACS Nano* **2011**, *5*, 968–974.
21. Hernandez, Y.; Nicolosi, V.; Lotya, M.; Blighe, F. M.; Sun, Z.; De, S.; McGovern, I. T.; Holland, B.; Byrne, M.; Gun'Ko, Y. K.; et al.

High-yield Production of Graphene by Liquid-phase Exfoliation of Graphite. *Nat. Nanotechnol.* **2008**, *3*, 563–568.
22. Vo, T. H.; Shekhirev, M.; Kunkel, D. A.; Morton, M. D.; Berglund, E.; Kong, L.; Wilson, P. M.; Dowben, P. A.; Enders, A.; Sinitskii, A. Large-scale Solution Synthesis of Narrow Graphene Nanoribbons. *Nat. Commun.* **2014**, *5*, 3189.
23. Chen, L.; Hernandez, Y.; Feng, X.; Müllen, K. From Nanographene and Graphene Nanoribbons to Graphene Sheets: Chemical Synthesis. *Angew. Chem., Int. Ed.* **2012**, *51*, 7640–7654.
24. Yan, X.; Cui, X.; Li, B.; Li, L.-s. Large, Solution-Processable Graphene Quantum Dots as Light Absorbers for Photovoltaics. *Nano Lett.* **2010**, *10*, 1869–1873.
25. Liu, C.; Yu, Z.; Neff, D.; Zhamu, A.; Jang, B. Z. Graphene-Based Supercapacitor with an Ultrahigh Energy Density. *Nano Lett.* **2010**, *10*, 4863–4868.
26. Xiao, J.; Mei, D.; Li, X.; Xu, W.; Wang, D.; Graff, G. L.; Bennett, W. D.; Nie, Z.; Saraf, L. V.; Aksay, I. A.; et al. Hierarchically Porous Graphene as a Lithium–Air Battery Electrode. *Nano Lett.* **2011**, *11*, 5071–5078.
27. Feng, X.-M.; Li, R.-M.; Ma, Y.-W.; Chen, R.-F.; Shi, N.-E.; Fan, Q.-L.; Huang, W. One-Step Electrochemical Synthesis of Graphene/Polyaniline Composite Film and Its Applications. *Adv. Funct. Mater.* **2011**, *21*, 2989–2996.
28. Cao, X.; Shi, Y.; Shi, W.; Lu, G.; Huang, X.; Yan, Q.; Zhang, Q.; Zhang, H. Preparation of Novel 3D Graphene Networks for Supercapacitor Applications. *Small* **2011**, *7*, 3163–3168.
29. Zhang, L.; Zhang, F.; Yang, X.; Long, G.; Wu, Y.; Zhang, T.; Leng, K.; Huang, Y.; Ma, Y.; Yu, A.; et al. Porous 3D Graphene-Based Bulk Materials with Exceptional High Surface Area and Excellent Conductivity for Supercapacitors. *Sci. Rep.* **2013**, *3*, 1408.
30. Tao, Y.; Xie, X.; Lv, W.; Tang, D.-M.; Kong, D.; Huang, Z.; Nishihara, H.; Ishii, T.; Li, B.; Golberg, D.; et al. Towards Ultrahigh Volumetric Capacitance: Graphene Derived Highly Dense but Porous Carbons for Supercapacitors. *Sci. Rep.* **2013**, *3*, 2975.
31. Mao, S.; Lu, G.; Chen, J. Three-Dimensional Graphene-Based Composites for Energy Applications. *Nanoscale* **2015**, *7*, 6924–6943.
32. Luo, B.; Zhi, L. Design and Construction of Three Dimensional Graphene-Based Composites for Lithium Ion battery Applications. *Energy Environ. Sci.* **2015**, *8*, 456–477.
33. Tucker Iii, C. L.; Moldenaers, P. Microstructural Evolution in Polymer Blends. *Annu. Rev. Fluid Mech.* **2002**, *34*, 177–210.
34. Lopez-Barron, C. R.; Macosko, C. W. Coarsening of PS/SAN Blends with Cocontinuous Morphology Studied with 3D Image Analysis. *Macromol. Symp.* **2009**, *283–284*, 348–353.
35. Trifkovic, M.; Hedegaard, A.; Huston, K.; Sheikhzadeh, M.; Macosko, C. W. Porous Films *via* PE/PEO Cocontinuous Blends. *Macromolecules* **2012**, *45*, 6036–6044.
36. Yuan, Z.; Favis, B. D. Coarsening of Immiscible Co-continuous Blends during Quiescent Annealing. *AIChE J.* **2005**, *51*, 271–280.
37. Prochazka, F.; Dima, R.; Majesté, J.; Carrot, C. Phase Inversion and Co-continuity Domain in Immiscible Polyethylene/Polystyrene Blends. *e-Polymers* **2013**, *3*, 512–522.
38. Paul, D. R.; Bucknall, C. B. *Polymer Blends: Formulation and Performance*; Wiley: New York, 1999; Vol. 1.
39. Galloway, J. A.; Macosko, C. W. Comparison of Methods for the Detection of Cocontinuity in Poly(ethylene oxide)/Polystyrene Blends. *Poly. Eng. Sci.* **2004**, *44*, 714–727.
40. Suzuki, T.; Murakami, Y.; Inui, T.; Takegami, Y. Morphological Study of Hydrophilic-Hydrophobic Polymer System by Inverse Gas Chromatography: Physical Blends of Poly(ethylene oxide) with Polystyrene. *Polym. J.* **1981**, *13*, 1027–1035.
41. Utracki, L. A.; Walsh, D. J.; Weiss, R. A. Polymer Alloys, Blends, and Ionomers—An Overview. *ACS Symp. Ser.* **1989**, *395*, 1–35.
42. Agarwala, R. C.; Agarwala, V. Electroless Alloy/Composite Coatings: A Review. *Sadhana* **2003**, *28*, 475–493.
43. Sudagar, J.; Lian, J.; Sha, W. Electroless Nickel, Alloy, Composite and Nano Coatings—A Critical Review. *J. Alloys Compd.* **2013**, *571*, 183–204.
44. Yan, Z.; Ma, L.; Zhu, Y.; Lahiri, I.; Hahm, M. G.; Liu, Z.; Yang, S.; Xiang, C.; Lu, W.; Peng, Z.; et al. Three-Dimensional Metal–Graphene–Nanotube Multifunctional Hybrid Materials. *ACS Nano* **2012**, *7*, 58–64.
45. Zhu, Y.; Li, L.; Zhang, C.; Casillas, G.; Sun, Z.; Yan, Z.; Ruan, G.; Peng, Z.; Raji, A.-R. O.; Kittrell, C.; et al. A Seamless Three-Dimensional Carbon Nanotube Graphene Hybrid Material. *Nat. Commun.* **2012**, *3*, 1225.
46. Xia, J.; Chen, F.; Li, J.; Tao, N. Measurement of the Quantum Capacitance of Graphene. *Nat. Nanotechnol.* **2009**, *4*, 505–509.
47. Jiang, L.; Fan, Z. Design of Advanced Porous Graphene Materials: From Graphene Nanomesh to 3D Architectures. *Nanoscale* **2014**, *6*, 1922–1945.